ACS OMEGA

Open Access

http://pubs.acs.org/journal/acsodf

Article

Physicochemical Properties of Seed Oil Blends and Their Potential for the Creation of Synthetic Oleosomes with Modulated Polarities

Brett A. Berger, Henry M. Vietor, Dane W. Scott, Hwayoung Lee, Sanaz Hashemipour, Wonpil Im, Nathan J. Wittenberg,* and Kerney Jebrell Glover*

Cite This: *ACS Omega* 2024, 9, 43193−43202

Read Online

ACCESS | Metrics & More | Article Recommendations | Supporting Information

ABSTRACT: There is an increasing demand within the pharmaceutical and cosmetic industries for biofriendly lipid-based active ingredient delivery systems. Micelles, liposomes, and lipid nanoparticles are currently the most used systems despite their limitations. Oleosomes, also known as lipid droplets, are promising alternatives to the existing strategies. Oleosomes are typically found in plant cells and are characterized by a nonpolar triacylglycerol core surrounded by a phospholipid monolayer punctuated with the protein oleosin. Producing oleosomes synthetically allows the customization of their lipid content, size, protein content, and oil core characteristics, expanding their versatility. Herein we demonstrate a proof of concept for the use of synthetic oleosomes to sequester polar molecules by modulating their core polarity with blends of sunflower and castor oils. The physical properties (density, refractive index, and permittivity) of the oil blends are characterized and demonstrate ideal mixing of the oils, which is supported by molecular dynamics simulations. Spectroscopic examination of the oil blends using fluorescent probes shows that the polarity of oil blends increases as the fraction of castor oil increases. Finally, we show that the uptake of a polar fluorescent probe (NBD-glucose) into synthetic oleosomes is enhanced by increasing the polarity of the oil core, but large charged molecules are excluded from the core regardless of polarity. These experiments show that synthetic oleosomes with tunable oil cores can expand the range of molecules that can be loaded into a biofriendly package as desired for biotechnology applications.

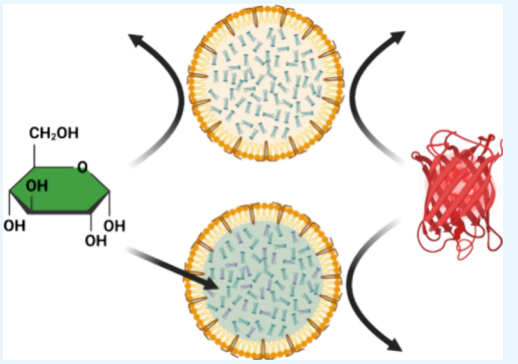

INTRODUCTION

Within the personal care and pharmaceutical industry there is great interest in the delivery of active ingredients using biofriendly lipid-based strategies.[1,2] Currently the primary methods of choice are micelles, liposomes and lipid nanoparticles. The simplest of these is the micelle.[3] Micelles are aggregates made of amphipathic detergent or lipid molecules that arrange with their hydrophobic tails inward and their hydrophilic heads outward. While touting easy assembly, micelles have a limited volume of cargo that they are able to hold due to their small size and can rapidly disintegrate if diluted below their critical micelle concentration.[4,5] Liposomes are composed of a spherical phospholipid bilayer with a central aqueous core which provides both hydrophilic and hydrophobic environments, thus expanding the range of molecules they can sequester.[6−10] However, liposomal sequestration of molecules is limited by cargo leakage and poor structural integrity. Lipid nanoparticles consist of a phospholipid monolayer that surrounds a liquid-crystalline lipid core. However, the final efficacy of delivery can be reduced due to alterations sustained during the high-pressure particle formation process or temperature-related changes to the fluidity of the solid core.[11,12]

Recently, oleosomes, also known as lipid droplets (LDs) or oil bodies, have emerged as a potentially superior delivery agent.[3,13−17] They are found in plant seeds where they function mainly as repositories of energy. Oleosomes have a well-established structure consisting of a triacylglycerol core encased by a phospholipid monolayer (Figure 1A).[18] The surface of oleosomes is punctuated extensively with the protein oleosin, which is thought to stabilize them.[18] Although oleosomes can be obtained directly from plant seeds, these naturally derived oleosomes lack customizability to meet the needs of specific applications as the size, phospholipid composition, protein content, and oil core characteristics are not easily altered.

On the other hand, synthetically prepared oleosomes have the potential to overcome the aforementioned limitations.[19,20] Recently, a new method was developed to create oleosomes of specific size, defined phospholipid composition, variable oleosin content, and tunable buoyancy.[21] However, the extremely hydrophobic properties of the triacylglycerol core limits the utility of oleosomes as only uniformly nonpolar molecules can

Received: August 14, 2024
Revised: September 27, 2024
Accepted: October 4, 2024
Published: October 11, 2024

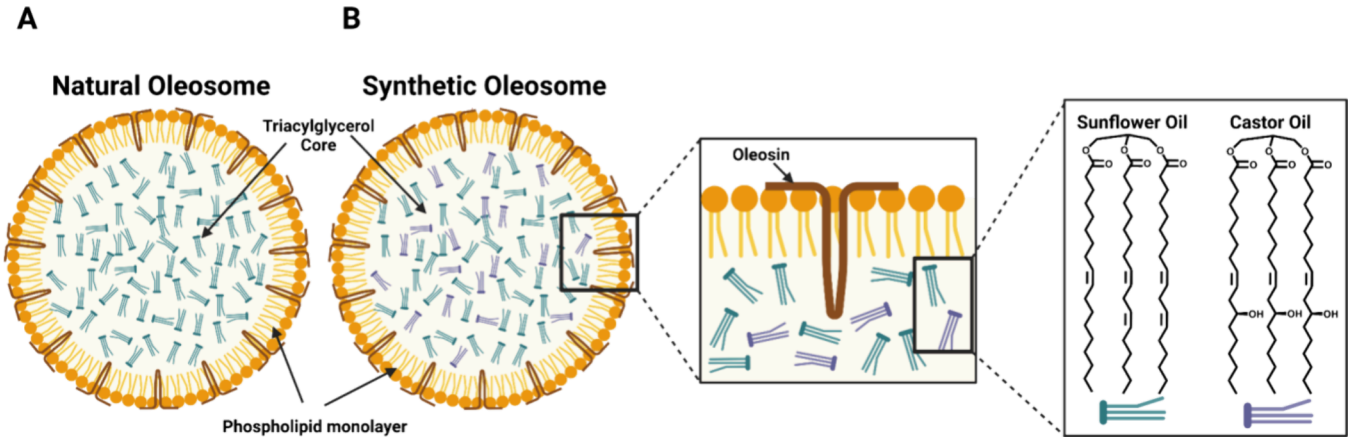

Figure 1. Cartoon depicting oleosome structure including oleosin inserted into the monolayer. (A) Natural oleosome. (B) Synthetic oleosome. CO molecules shown in teal. SO molecules shown in purple.

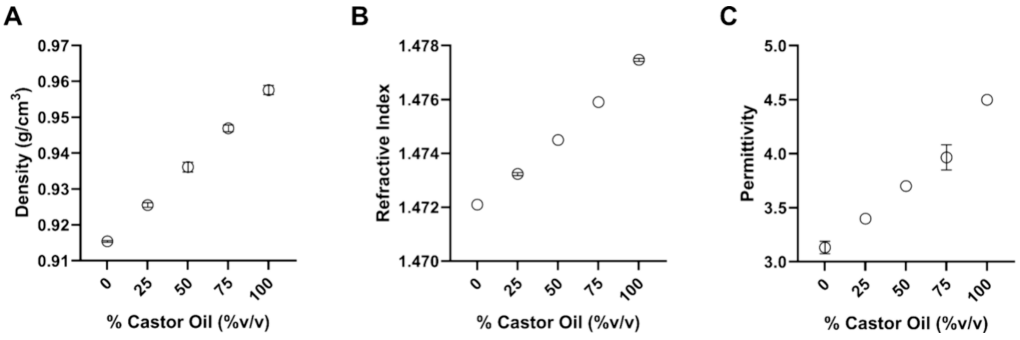

Figure 2. Physicochemical properties of oil blends. (A) Density. (B) Refractive index. (C) Permittivity. Mean of 3 trials plotted with standard deviation (deviation of 0 results in no plotted bars).

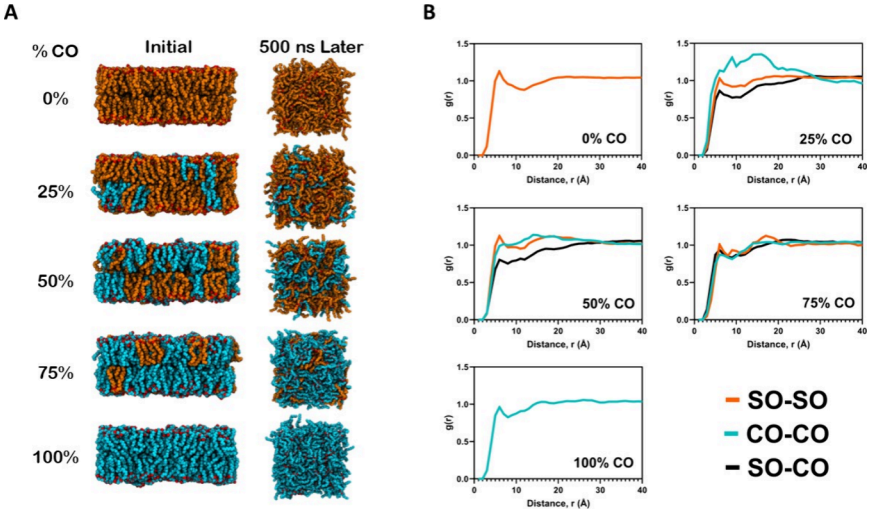

Figure 3. (A) MD simulation snapshots of oil blends at 0 ns (initial) and 500 ns. Sunflower oil (SO) and castor oil (CO) are shown in orange and cyan, respectively. (B) Radial distribution functions $g(r)$ of oil blends. Cyan, orange, and black traces are CO−CO, SO−CO, and SO−CO interactions, respectively. The central oxygen atom in the glycerol backbone of the triacylglycerol was used to calculate distances.

be sequestered. To render oleosomes more amenable to uptaking molecules which are more polar, we have created synthetic oleosomes with a core that is a blend of sunflower oil and castor oil (Figure 1B). We demonstrate that by modulating the core polarity of our oleosomes using the more polar castor oil, the selective uptake of glucose, a polar molecule, is improved without affecting the ability of the oleosome membrane to exclude soluble proteins from entering. We believe the experiments reported herein serve as a proof of concept for using modulated core properties to expand the application of oleosomes for molecule sequestration.

RESULTS AND DISCUSSION

Physicochemical Properties of Oil Blends. Sunflower oil (SO) and castor oil (CO) possess the typical triacylglycerol structure aside from the fact that CO employs ricinoleic acid, an

https://doi.org/10.1021/acsomega.4c07512
ACS Omega 2024, 9, 43193−43202

unusual fatty acid that contains hydroxyl groups making CO more polar relative to SO (Figure 1B). Therefore, the polarity of the oil blend can be modulated via the volume fraction of CO. To characterize the physical properties of these blends several quantities were measured: density, refractive index, and permittivity. The density is expected to increase as the percentage of CO increases, as CO is more dense than SO due to the presence of hydroxyl groups on the fatty acid tails. This trend was observed, and the oil blends demonstrated a positive linear trend as the percentage of CO increases (Figure 2A). The refractive index also increases linearly with the increase in the volume fraction of CO as CO has a higher refractive index than SO (Figure 2B). The dielectric constant or permittivity of the blends also increased linearly with an increasing percentage of CO, indicating that the overall polarity of the blend was increasing (Figure 2C). Although CO increases the density of the oil blend, at all percentages of CO, the density remains less than that of water, indicating that these mixtures, when formed into oleosomes, will still rise to the top of an aqueous medium. Taken together, the linearity of the trends as the volume fraction of CO increases strongly supports that the two oils are mixing ideally.

Molecular Dynamics Simulations of Oil Blends. To study the mixing behavior of the oil blends further, molecular dynamics (MD) simulations were employed. For each percentage of CO, 5 replicates were simulated, with each initially having a unique randomly distributed placement of SO and CO molecules. The systems were allowed to equilibrate over 500 ns to see if any segregation of SO or CO molecules occurred. The initial and final simulation snapshots are shown in Figure 3A. Due to the constraints of the Membrane Builder framework, initially the CO and SO are placed in a bilayered configuration. However, as the simulations proceeded, the bilayer structure disappeared allowing the SO and CO molecules to mix freely. As a consequence, by the end of the simulation at 500 ns, the dimensions of the system box became a square as opposed to its initial rectangular shape. Similar behavior has been seen in lipid bilayer simulation studies containing significant fractions of triacylglycerol lipids.[22−24] Importantly, during the simulation, SO and CO appear to mix freely (i.e., not showing a preference based on its initial positioning in the replicate) regardless of the percentage of CO (Sup. Video 1).

Next, radial distribution functions (RDFs) were calculated to quantitate the degree of mixing between SO and CO molecules (Figure 3B). The RDF, denoted as $g(r)$, quantifies the probability of finding a lipid at a distance r from a reference lipid compared to that of a random distribution. Therefore, a $g(r)$ equal to one indicates a random (i.e., homogeneous) distribution, while a $g(r)$ that deviates significantly from 1 indicates lipid segregation. For all percentages of CO, $g(r)$ was a relatively flat curve which remained close to 1 over the entire system box, which indicates homogeneous mixing of SO and CO in the oil blends. Lastly, system density was calculated (Sup. Figure 1). The positive linear trend as a function of percentage of CO agrees well with the density data shown in Figure 2A. Although the trend agrees well with the experimental data, the absolute densities are slightly lower than the experimental values perhaps due to limitations of the force field employed in the simulations. Overall, the MD simulation results reinforced the experimental data showing that the mixing CO and SO appears to be ideal (i.e., lipids not showing a preference to associate with themselves).

Interaction of Fluorescent Probes with Oil Blends. Three different hydrophobic fluorescent probes (Prodan, curcumin, and pyrene) were used to study the chemical properties of the oil blends (Figure 4). Prodan contains only

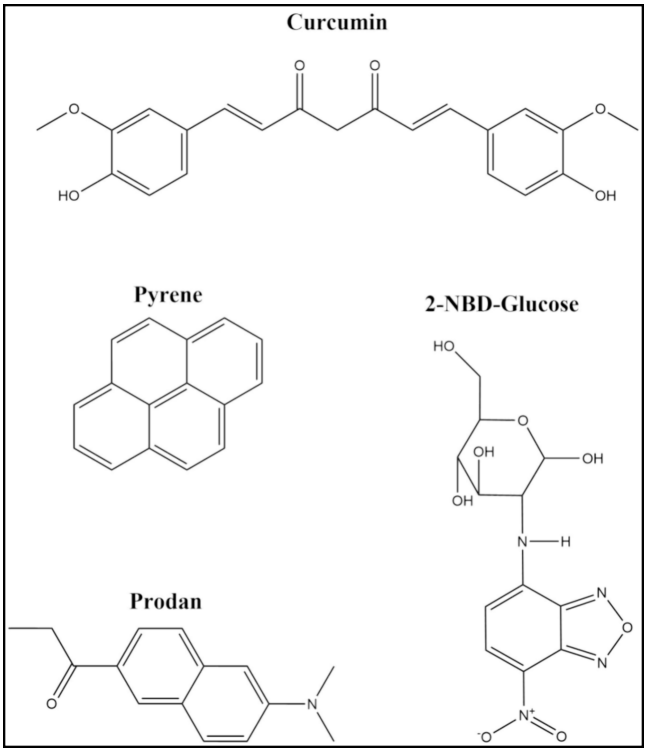

Figure 4. Chemical structures of fluorescent probes.

hydrogen bond acceptor sites, while curcumin can both donate and accept hydrogen bonds. Pyrene, can neither donate nor accept hydrogen bonds. Both Prodan and curcumin are solvatochromic, meaning that their wavelength of maximum emission (λ_{max}) is responsive to the polarity of the environment (Sup. Figure 2). Both Prodan and curcumin demonstrate a red shift in λ_{max} as the volume fraction of CO increases (Figure 5). This shift is expected as CO is more polar than SO. This finding is consistent with the previously discussed observation that CO has a higher permittivity than SO.

Interestingly, the λ_{max} of Prodan and curcumin in the oil blends did not increase linearly as was to be expected based on the permittivity (Figure 2C). Instead, the maximum emission wavelength increased rapidly upon the initial addition of CO before leveling off as the mixture came closer to being entirely

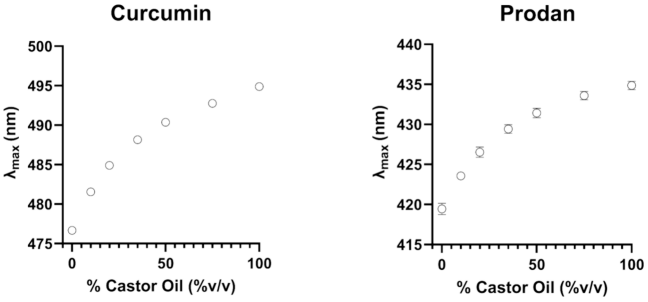

Figure 5. Change in λ_{max} of fluorescent probes as a function of oil concentrations.

https://doi.org/10.1021/acsomega.4c07512
ACS Omega 2024, 9, 43193−43202

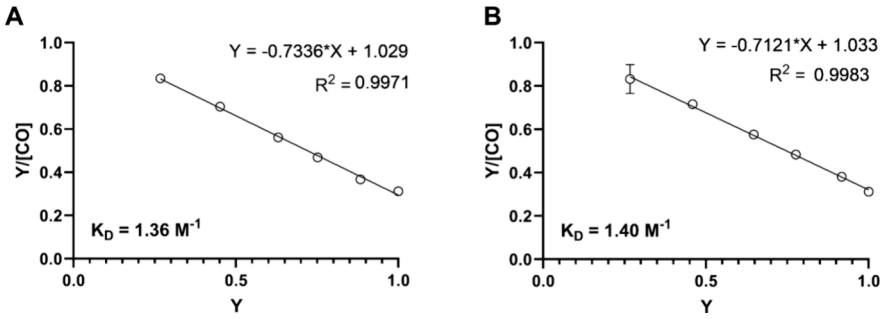

Figure 6. Scatchard plot of fluorescent probes as a function of oil concentrations. (A) Curcumin. (B) Prodan.

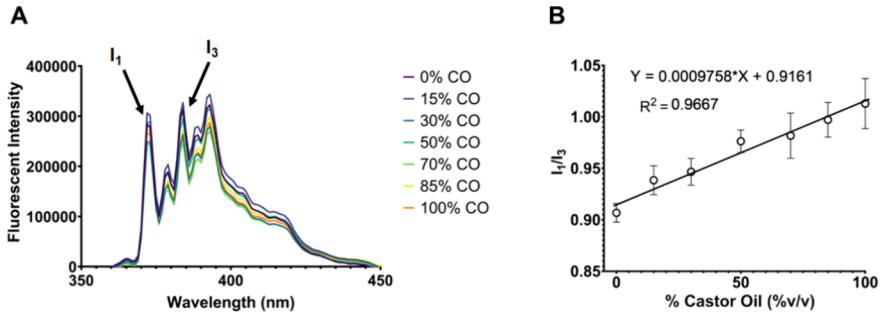

Figure 7. (A) Fluorescence spectrum of pyrene as a function of oil concentration. (B) Linear regression analysis of I_1/I_3 for pyrene in various oil blends.

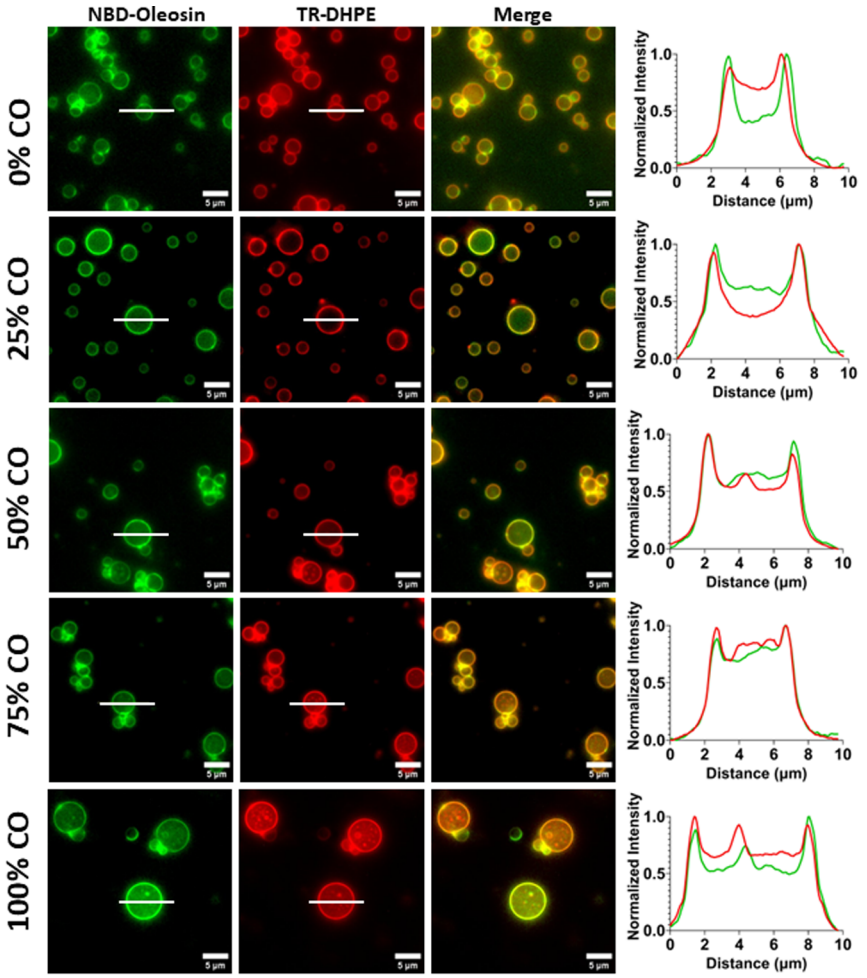

Figure 8. Fluorescence images of NBD-oleosin (green) and TR-DHPE (red) embedded in lipid monolayer.

https://doi.org/10.1021/acsomega.4c07512
ACS Omega 2024, 9, 43193−43202

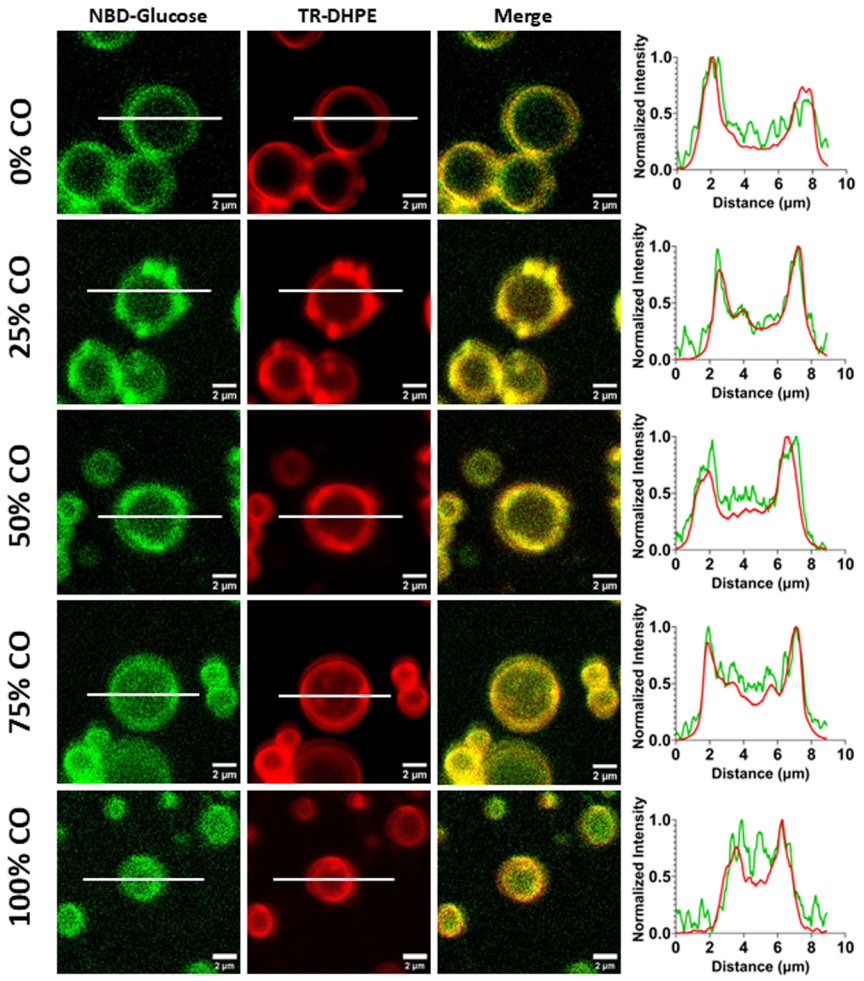

Figure 9. Fluorescence images of NBD-glucose (green) in TR-DHPE-labeled (red) synthetic oleosomes.

CO (Figure 5). This nonlinear trend shows that Prodan and curcumin possess a preference for the more polar CO over the less polar SO.

These findings were further analyzed via Scatchard analysis (Figure 6) where the value Y represents the fraction of CO molecules behaving as if they were in a 100% CO environment. The K_D values for Prodan and curcumin were found to be 1.40 M^{-1} and 1.36 M^{-1} respectively, indicating a measurable but weak preference for CO to SO. The x-intercept of the Scatchard plot provides further information, as it is equivalent to the number of CO molecules bound to each probe. Prodan was found to bind to 1.45 CO molecules, while curcumin was found to bind to 1.40 CO molecules. These values indicate that each probe can interact with multiple CO molecules, most likely through their hydrogen bond donating and/or accepting sites.

To determine the role of hydrogen bonding in the interactions between the probes and the oil blends, we chose a third fluorophore, pyrene, which can neither donate nor accept hydrogen bonds. Pyrene lacks the broad emission spectrum and solvatochromism displayed by Prodan and curcumin. Pyrene's emission spectrum instead consists of five unique peaks, denoted as I_1 through I_5 (Figure 7A). Peak I_1 has been shown to increase in intensity relative to I_3 as solvent polarity increases, making the ratio of the intensity of peak I_1 to peak I_3 a metric for understanding how the polarity of the oil blend changes.[25] This ratio, when plotted against the volume fraction of CO, demonstrated a linear relationship (Figure 7B), which is consistent with the permittivity of the oil blends, and strongly suggests that hydrogen bonding is the main contributor to the preference of CO over SO for Prodan and curcumin.

Synthetic Oleosomes Containing Oil Blends. Now that we characterized the oil blends, we sought to investigate the possibility of creating synthetic oleosomes with them using the methodology that was previously established in our lab.[21] For these studies, the synthetic oleosomes were prepared with biotin-PE in their lipid monolayer so that they would adhere to a neutravidin-coated glass surface. This immobilization scheme allowed the oleosomes to remain on the surface of the glass instead of floating away due to their low density. A hallmark of successfully prepared oleosomes is an intact outer lipid monolayer, punctuated with the oleosin protein. As seen in Figure 8, for all volume fractions of CO, the signal from the red (TR-DHPE) channel, which marks the lipid monolayer, and the green (NBD-oleosin) channel strongly colocalize around the perimeter of the synthetic oleosomes, indicating synthetic oleosomes can be prepared using CO and SO blends. The intensity line scans in Figure 8 further confirm that TR-DHPE and NBD-oleosin colocalize on the perimeter of the synthetic oleosomes. In addition, we measured the diameters of synthetic oleosomes as a function of their CO content. For a fixed total oil-to-phospholipid ratio, the diameters of the synthetic oleosomes were not different, regardless of the CO fraction (Sup. Figure 3) showing the oil blends do not affect the fundamental properties of the oleosomes.

https://doi.org/10.1021/acsomega.4c07512
ACS Omega 2024, 9, 43193−43202

As the volume fraction of CO in the synthetic oleosomes increased, we observed substructures within the oil cores. We were able to identify the composition of these substructures using a lipophilic fluorophore (i.e., BODIPY). Clearly from Sup. Figure 4 the BODIPY does not enter the substructure, indicating that the composition is highly polar and thus water-based. In addition, the presence of a TR-DHPE signal reveals that these water substructures possess a monolayer in which the tails of the monolayer point into the oil core and the polar heads toward the water substructure. These likely form during the oleosome self-assembly process due to the increased solubility of water in the oil phase as the volume fraction of CO increases.

Uptake of NBD-Glucose in Synthetic Oleosomes with CO-Rich Cores. Next, we sought to investigate the ability to selectively sequester a molecule inside the oil core as a function of the volume fraction of CO. Fluorescently labeled glucose (Figure 4) was chosen because it is highly polar and is not expected to enter the oil core of a traditional oleosome. Figure 9 shows representative confocal microscopy images of our synthetic oleosomes in the presence of NBD-glucose. In the 0% CO trials, the NBD-glucose minimally enters the core of the synthetic oleosomes. However, it appears that the NBD-glucose interacts with the perimeter of the oleosome. As the volume fraction of CO increases, the NBD-glucose begins to enter the core. The intensity line scans in Figure 9 clearly show that as the volume fraction of CO increases, the NBD-glucose fluorescence becomes significantly more intense in the oleosome core. Figure 10 shows the strong correlation between NBD-glucose fluorescence and volume fraction of CO. This increased intensity is not adulterated by out-of-focus fluorescence, because our synthetic oleosomes (~5 μm diameter) are significantly larger than the confocal focal plane thickness (<1 μm) which keeps the inclusion of out-of-focus fluorescence to a minimum. In addition, the substructures observed in synthetic oleosomes with high concentrations of CO (Sup. Figure 4), also do not result in the artificial increase in NBD-glucose fluorescence intensity observed as the substructures are not visualized as bright spots of NBD-glucose fluorescence (Figure 9) and the interior intensity of the NBD-glucose containing synthetic oleosomes is relatively uniform (i.e., not punctuated). It is possible that differences in the size of the synthetic oleosomes or slightly nonequatorial focusing of the images may contribute to variances in the total fluorescence intensity; however, as seen in Supp. Figure 3, there is no significant difference in synthetic oleosome size as a function of the CO concentration and combined with sufficient sampling of the synthetic oleosomes for each concentration (>40 oleosomes), variance from all sources is minimized. Thus, the trend of increasing interior fluorescent intensity from NBD-glucose as a function of CO concentration is in fact caused by the modulated core polarity and this demonstrates the viability of tuning the polarity of the oil core to modulate the uptake of a particular molecule.

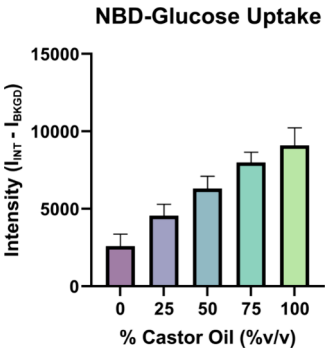

Figure 10. Background-corrected fluorescence intensity of NBD-glucose in synthetic oleosomes with varying concentrations of CO in their core.

Charged Proteins Are Excluded from Synthetic Oleosomes. Lastly, we wanted to confirm that by changing the core polarity, the oleosomes have not lost their ability to exclude highly charged molecules. mCherry is a highly charged fluorescent protein that should not pass through the lipid monolayer and be sequestered in the core, regardless of the core polarity. Figure 11 shows representative fluorescence images of all core composition ratios. The use of NBD-oleosin allows for the determination of the edge of the oleosomes. In the mCherry fluorescence channel, there is uniform red signal except for where the oleosomes are located. Clearly, mCherry cannot pass through the lipid monolayer and enter into the core of the synthetic oleosomes. The line scans confirm that there is high intensity of mCherry outside of the oleosomes but very little signal inside. Thus, regardless of core polarity, the entering of highly charged particles into the core is not observed.

CONCLUSIONS

There is increasing interest in using oleosomes for cosmetic, pharmaceutical, and industrial applications based on their ability to encapsulate molecules in the droplet's oil core. Most natural oleosomes are composed of highly nonpolar triacylglycerols, which limits the types of molecules that they can sequester. Herein, we have demonstrated a new approach to synthetic oleosome design. These synthetic oleosomes are stabilized by oleosin, have a predictable size, and have a tunable core for the sequestration of compounds with more polar characteristics. We found that by changing the ratio of SO to CO in the core of the synthetic oleosomes, the propensity for NBD-glucose to enter the core could be modulated. We have also demonstrated through simulations that the two oils mix in ideally and uniformly within the synthetic oleosomes. The tuning of the core did not affect the ability of the oleosome to prevent charged proteins from entering into the core. Selectively controlling the polarity (or conceivably other properties) of the core greatly expands the utility of synthetic oleosomes for industrial applications.

MATERIALS AND METHODS

Reagents and Chemicals. Sunflower oil and castor oil were purchased from Sigma-Aldrich and Alfa Aesar, respectively. Egg PC was obtained from Avanti Polar Lipids. 2-NBD-glucose and curcumin were purchased from Cayman Chemical Company. Pyrene was purchased from Thermo Scientific, and Prodan was purchased from TCI America. All chemicals were of standard ACS grade. Oleosin was expressed and purified to homogeneity as described previously.[26]

Determination of Refractive Indices of Oil Blends. Samples of the oil blends with 1 mL total volume were prepared by adding the needed volumes of sunflower oil and castor oil to produce 100, 75, 50, 25, and 0% v/v sunflower oil blends. The samples were then heated in a hot water bath and mixed. 300 μL of an oil blend was added to the stage of an Anton Paar Abbemat 3200 refractometer, allowed to reach 25 °C, and then measured. The oil was then removed from the stage, which was subsequently cleaned with ethanol. This process was repeated

https://doi.org/10.1021/acsomega.4c07512
ACS Omega 2024, 9, 43193−43202

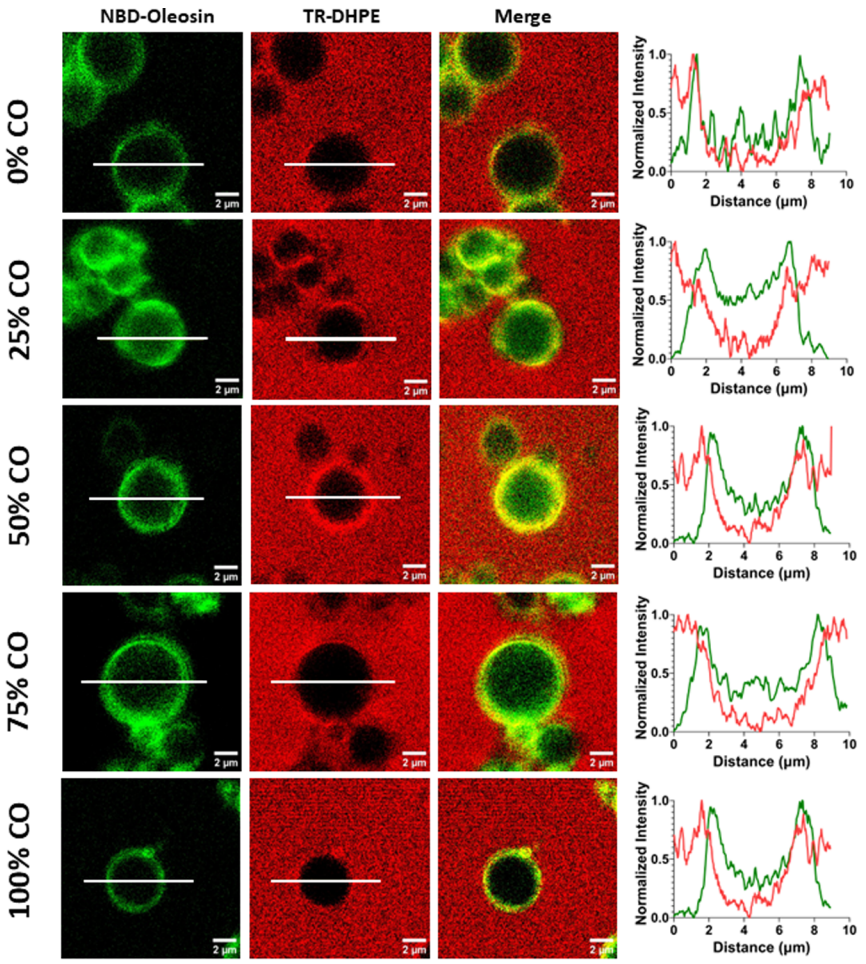

Figure 11. Fluorescence images of synthetic oleosomes with NBD-oleosin (green) that exclude mCherry (red).

in triplicate for all samples, ensuring the stage was thoroughly cleaned in between trials. The refractometer was calibrated with distilled water.

Determination of Densities of Oil Blends. Sunflower oil and castor oil blends (1.6 mL total volume) were prepared in the same volume ratios as for the determination of the refractive index. The Kyoto Electronics DA-210 density/specific gravity meter was prepared by first cleaning the density meter thoroughly with a solution of 5 g of dish soap containing sodium dodecyl sulfate and 3 g of sodium bicarbonate in 100 mL of water. Following cleaning, the density meter was rinsed thoroughly with deionized water before being dried with nitrogen gas for 3 min. The density meter was then calibrated using air and ultrapure water. Following calibration, the oil samples were drawn into syringes and injected into the density meter, ensuring no bubbles entered the loop. Following each measurement, the density meter was cleaned using the previously described detergent solution, rinsed with water, and dried with nitrogen for 3 min. All measurements were performed in triplicate.

Determination of Permittivity of Oil Blends. A dielectric meter, BI 870, from Brookhaven Instruments was used for the measurement of oils and blends. The meter was calibrated to read the literature reported permittivity of *n*-hexane at 25 °C, which is 1.9. Once a stable reading was obtained, the measurement probe was drained of *n*-hexane and then immersed in an oil sample. The oil sample was in a 25 mL glass cylindrical tube clamped in place such that the oil inside the cylinder was level with the water in a circulating temperature controlled bath. After each measurement, the probe was removed, the oil was drained and the probe was thoroughly rinsed with *n*-hexane. The probe was then placed in pure *n*-hexane to ensure calibration before the next oil blend measurement. Three independent samples of each oil blend were measured.

Spectroscopy of Fluorescent Probes in Oil Blends. Fluorescence spectroscopy of castor oil and sunflower oil mixtures was performed using a Tecan Infinite Nano Pro. Samples were prepared by first adding 10 μL of sunflower oil (except for the 100% castor oil sample, where 10 μL of castor oil was added instead), followed by 50 μL of chloroform and 1.5 μL of a 2 mM fluorescent probe (Prodan, curcumin, or pyrene) solution in chloroform. The samples were then vortexed and placed under a stream of dry nitrogen gas for 10 min each. Following drying, the samples were centrifuged for 1 min to collect the oil in the bottom of the tube. The blends were then completed by adding the volume of each oil needed to achieve a total volume 200 μL per sample of the desired sunflower oil to castor oil ratio. Samples without the fluorescent molecule were prepared by adding the volume of oil needed to make 200 μL samples of the desired oil ratio to a separate tube. 100 μL of all samples were then added to a black polystyrene 96-well plate before being placed into the Tecan Infinite Nano Pro. The gain was calculated from the 100% sunflower with the fluorescent molecule and all measurements were performed in triplicate. The blends with Prodan and curcumin were prepared via this method. Pyrene samples were prepared via the same process,

https://doi.org/10.1021/acsomega.4c07512
ACS Omega 2024, 9, 43193−43202

however, instead used ten times the volume of each component. These spectra were collected using a Horriba Fluorolog Fluorometer to make use of its superior bandwidth to discriminate the finer details of Pyrene's emission spectrum. The measurements, as with Prodan and curcumin, were performed in triplicate. For the Scatchard plots, Y was calculated using the equation:

$$Y = \frac{\lambda_{\max,\mathrm{obs}} - \lambda_{\max,100\%\mathrm{SO}}}{\lambda_{\max,100\%\mathrm{CO}} - \lambda_{\max,100\%\mathrm{SO}}}$$

where $\lambda_{\max,\mathrm{obs}}$ is the maximum emission wavelength for Prodan or curcumin in an oil blend, and $\lambda_{\max,100\%\mathrm{SO}}$ and $\lambda_{\max,100\%\mathrm{CO}}$ are the maximum emission wavelengths for Prodan or curcumin in 100% sunflower oil and castor oil, respectively.

MD Simulations of Oil Blends. All-atom MD simulations were prepared using the CHARMM36 lipid force field.[23,27] Five different systems composed of a total of 200 oil lipids (Sup. Table 1), either pure oil type (SO or CO) or oil mixture (SO and CO), were constructed using Membrane Builder in CHARMM-GUI (https://www.charmm-gui.org) with optimized TAG headgroup parameters with increased hydrophobicity.[23,28−32] Each system has 5 replicates for better trajectory sampling Initially, each system contained 150 mM KCl bulk ionic solution along with the TIP3P water model, but they were all removed manually by utilizing Input Generator's CHARMM script to build the corresponding oil blend systems without bulk water and ions.[33] For the production simulation, OpenMM 8.0 was utilized for all systems.[34] A force-based switching method was applied for van der Waals interactions between 10 and 12 Å and the particle-mesh Ewald method was used for long-range electrostatic interactions.[35] A temperature of 303.15 K was maintained by the Langevin dynamics with a 1 ps^{-1} of coupling frequency. Note that, instead of using a semi-isotropic barostat method ($X = Y \neq Z$) for typical membrane systems, the isotropic Monte Carlo barostat method ($X = Y = Z$) was used for the oil blend systems with the constant pressure at 1 bar.[36] All bonds containing hydrogen atoms were fixed by SHAKE algorithm and hydrogen mass repartitioning method was applied and a 4 fs time step was employed during the *NPT* (constant number of particles, pressure, and temperature) production run of 500 ns.[37,38] The last 100 ns of trajectories were used for analysis, and VMD program was used for the trajectory visualization.[39] The RDFs were calculated using the CHARMM rdfsol command.[40]

Oleosome Preparation. Synthetic oleosomes were prepared from egg PC, biotin-PE, sunflower oil, castor oil, and oleosin. The egg PC (10 mg/mL) and biotin-PE (0.1 mg/mL) were in a 99/1% molar ratio. The sunflower oil and castor oil were added based on the desired ratio of total volume in the core (14.6 μL). The mixture was then dissolved in 50 μL of chloroform and vortexed until homogeneous. The solvent was dried under nitrogen gas until fully dry. The sample was then dissolved in 3.5 mL of a high-salt buffer (10 mM Tris, 2.2 mM $CaCl_2$, 250 mM NaCl) and sonicated for 3.5 min using a Branson sonifier 450 equipped with a 3 mm diameter microtip (duty cycle, 10%; output power, 4). Oleosin was then added with a molar ratio of 50/1 egg PC/oleosin and sonicated for an additional 3.5 min. Finally, the oleosomes were filtered through Whatman grade 1 filter paper.

Surface Capture of Oleosomes. Neutravidin functionalized glass was used to capture the biotinylated oleosomes. Glass coverslips were washed with isopropanol, Milli-Q water, blown dry with nitrogen gas, and then soaked in 2% w/v sodium dodecyl sulfate (SDS) overnight until use. They were then washed with isopropanol, Milli-Q water, blown dry with nitrogen gas, and then exposed to UV-Ozone (ProCleaner Plus, Bioforce Nanosciences) for 30 min. The coverslips were then coated in a solution of 0.2 mg/mL Neutravidin for 20 min. Finally, they were washed with Milli-Q water and blown dry with N2. Immediately after the completion of the oleosome preparation, 1 mL aliquots were pipetted onto the bottom of a high walled washing container. The functionalized glass coverslips were placed functionalized side down onto the top of the oleosome aliquots and left for 5 min. The container was then filled with high-salt buffer. While staying fully submerged, the coverslips were mounted in Attofluor imaging chambers. Once assembled, the chambers could be removed from the washing container right side up to keep the oleosomes submerged.

Epifluorescence Microscopy. To perform initial characterization of the effect of core composition on the synthetic oleosome formation, they were imaged via epifluorescent microscopy. Fluorescence images were acquired with a Nikon Ti inverted microscope using a 100× objective with 1.49 numerical aperture. Fluorescence was excited with an Aura II LED light engine (Lumencor), and images were collected with a Hamamatsu Orca Flash 4.0 v2 sCMOS camera. The microscope system was controlled with Nikon Elements software. Fluorescent images were colored and analyzed in ImageJ. Line scans were plotted in GraphPad Prism 10.

Confocal Microscopy. To study the extent of the ability of the oleosomes to exclude or uptake chemicals based on the core composition, confocal microscopy was used. Fluorescent images were acquired with Nikon C2+ laser scanning confocal microscope using a 60× objective with 1.4 numerical aperture. Fluorescence was excited with a LU-N4 laser unit and detected via PMT. The microscope system was controlled with Nikon Elements software. Fluorescent images were colored and analyzed in ImageJ. Line scans were plotted in GraphPad Prism 10.

mCherry Exclusion Microscopy. To study the exclusion of mCherry for the synthetic oleosomes, NBD labeled oleosin was used in the above steps. After the assembly of the imaging chamber as described above, mCherry was added to achieve a final concentration of 500 nM mCherry. The chamber was incubated for 30 min and then imaged with confocal microscopy. Fluorescent images were colored and analyzed in ImageJ. Line scans were plotted in GraphPad Prism 10.

NBD-Glucose Uptake Microscopy. To study the uptake of NBD-Glucose, unlabeled oleosin was used. To visualize the edge of the oleosomes, TR-DHPE was added during the initial oleosome formation. The final molar ratio of lipids was 98/1/1% (Egg PC/Biotin-PE/TR-DHPE). After the assembly of the imaging chamber as described above, NBD-Glucose was added to each chamber to achieve a final concentration of 100 μM NBD-Glucose. The sample was incubated for 30 min and then washed thoroughly with high-salt buffer. The sample was then imaged with confocal microscopy. Using ImageJ, the average interior intensity of the synthetic oleosomes were measured using the circular ROI tool. For each image, an average background intensity was also measured. Then, the difference between the mean intensity of the synthetic oleosomes and the mean intensity of the background was calculated and plotted in GraphPad Prism 10. Data are reported as the average ∓ standard deviation for each percentage of CO. At least 40 synthetic oleosomes were measured for each condition.

https://doi.org/10.1021/acsomega.4c07512
ACS Omega 2024, 9, 43193−43202

■ ASSOCIATED CONTENT

Supporting Information

The Supporting Information is available free of charge at https://pubs.acs.org/doi/10.1021/acsomega.4c07512.

Density of oil blends from MD simulations, fluorescence spectra of Prodan and curcumin, diameters of synthetic oleosomes as a function of oil core composition, additional fluorescence micrographs of synthetic oleosomes, and a table of the oil blend compositions used for MD simulations (PDF)

Movie of a MD simulation trajectory for a blend of sunflower and castor oils (MP4)

■ AUTHOR INFORMATION

Corresponding Authors

Nathan J. Wittenberg − *Department of Chemistry, Lehigh University, Bethlehem, Pennsylvania 18015, United States;* orcid.org/0000-0001-9196-1867; Phone: (610)-759-5081; Email: njw@lehigh.edu; Fax: (610)-758-6536

Kerney Jebrell Glover − *Department of Chemistry, Lehigh University, Bethlehem, Pennsylvania 18015, United States;* orcid.org/0000-0002-1867-4965; Phone: (610)-759-5081; Email: kjg206@lehigh.edu; Fax: (610)-758-6536

Authors

Brett A. Berger − *Department of Chemistry, Lehigh University, Bethlehem, Pennsylvania 18015, United States;* orcid.org/0009-0001-6641-2003

Henry M. Vietor − *Department of Chemistry, Lehigh University, Bethlehem, Pennsylvania 18015, United States*

Dane W. Scott − *Department of Chemistry, East Tennessee State University, Johnson City, Tennessee 37614, United States;* orcid.org/0000-0003-0018-7189

Hwayoung Lee − *Department of Biological Sciences, Lehigh University, Bethlehem, Pennsylvania 18015, United States;* orcid.org/0000-0003-2332-1993

Sanaz Hashemipour − *Department of Chemistry, Lehigh University, Bethlehem, Pennsylvania 18015, United States*

Wonpil Im − *Departments of Biological Sciences and Bioengineering, Lehigh University, Bethlehem, Pennsylvania 18015, United States;* orcid.org/0000-0001-5642-6041

Complete contact information is available at: https://pubs.acs.org/10.1021/acsomega.4c07512

Notes

The authors declare no competing financial interest.

■ ACKNOWLEDGMENTS

Figure 1 and the TOC graphic were created using BioRender.com, but no templates were used in the production. This work was supported by NSF 2203362 awarded to K.J.G., N.J.W., and W.I. and NSF MCB-2111728 to W.I.

■ REFERENCES

(1) Vellu, J. P.; Nasir, H. M.; Setapar, S. H. M.; Ahmad, A.; Chuo, S. C.; Alshammari, M. B. Insights into the Application of Reverse Micelles in Cosmetic Formulations: A Review: Journal of Cosmetic Science. *J. Cosmet. Sci.* **2022**, *73* (5), 329−344.

(2) Vushakola, P.; Sailaja, A. K. Microemulsions - A Potential Carrier for Drug Delivery. *Innovare J. Life Sci.* **2016**, *6*, 1−5.

(3) Torchilin, V. P. Lipid-Core Micelles for Targeted Drug Delivery. *Curr. Drug Delivery* **2005**, *2* (4), 319−327.

(4) Jones, M.-C.; Leroux, J.-C. Polymeric Micelles−a New Generation of Colloidal Drug Carriers. *Eur. J. Pharm. Biopharm.* **1999**, *48* (2), 101−111.

(5) Sahib, M. N.; Abdulameer, S. A.; Darwis, Y.; Peh, K. K.; Tan, Y. T. F. Solubilization of Beclomethasone Dipropionate in Sterically Stabilized Phospholipid Nanomicelles (SSMs): Physicochemical and in Vitro Evaluations. *Drug Des. Devel. Ther.* **2012**, *6*, 29−42.

(6) Hua, S.; Wu, S. Y. The Use of Lipid-Based Nanocarriers for Targeted Pain Therapies. *Front. Pharmacol.* **2013**, *4*, 143.

(7) Ning, Y.-M.; He, K.; Dagher, R.; Sridhara, R.; Farrell, A. T.; Justice, R.; Pazdur, R. Liposomal Doxorubicin in Combination with Bortezomib for Relapsed or Refractory Multiple Myeloma. *Oncology* **2007**, *21* (12), 1503−1508. discussion 1511, 1513, 1516 passim

(8) Liu, P.; Chen, G.; Zhang, J. A Review of Liposomes as a Drug Delivery System: Current Status of Approved Products, Regulatory Environments, and Future Perspectives. *Molecules* **2022**, *27* (4), 1372.

(9) Mukherjee, A.; Bisht, B.; Dutta, S.; Paul, M. K. Current Advances in the Use of Exosomes, Liposomes, and Bioengineered Hybrid Nanovesicles in Cancer Detection and Therapy. *Acta Pharmacol. Sin.* **2022**, *43* (11), 2759−2776.

(10) Sercombe, L.; Veerati, T.; Moheimani, F.; Wu, S. Y.; Sood, A. K.; Hua, S. Advances and Challenges of Liposome Assisted Drug Delivery. *Front. Pharmacol.* **2015**, *6*, 286.

(11) Cárdenas, M.; Campbell, R. A.; Yanez Arteta, M.; Lawrence, M. J.; Sebastiani, F. Review of Structural Design Guiding the Development of Lipid Nanoparticles for Nucleic Acid Delivery. *Curr. Opin. Colloid Interface Sci.* **2023**, *66*, No. 101705.

(12) Akanda, M.; Mithu, M. S. H.; Douroumis, D. Solid Lipid Nanoparticles: An Effective Lipid-Based Technology for Cancer Treatment. *J. Drug Delivery Sci. Technol.* **2023**, *86*, No. 104709.

(13) Boucher, J.; Cengelli, F.; Trumbic, D.; Marison, I. W. Sorption of Hydrophobic Organic Compounds (HOC) in Rapeseed Oil Bodies. *Chemosphere* **2008**, *70* (8), 1452−1458.

(14) Hanano, A.; Almousally, I.; Shaban, M.; Rahman, F.; Blee, E.; Murphy, D. J. Biochemical, Transcriptional, and Bioinformatic Analysis of Lipid Droplets from Seeds of Date Palm (Phoenix Dactylifera L.) and Their Use as Potent Sequestration Agents against the Toxic Pollutant, 2,3,7,8-Tetrachlorinated Dibenzo-p-Dioxin. *Front. Plant Sci.* **2016**, *7*, 836.

(15) Bhardwaj, N.; Kundu, S. C. Electrospinning: A Fascinating Fiber Fabrication Technique. *Biotechnol. Adv.* **2010**, *28* (3), 325−347.

(16) *US-10863761-B2 - Methods and Compositions for Consumables | Unified Patents*. https://portal.unifiedpatents.com/patents/patent/US-10863761-B2 (accessed March 2024).

(17) Lipinski, C. A.; Lombardo, F.; Dominy, B. W.; Feeney, P. J. Experimental and Computational Approaches to Estimate Solubility and Permeability in Drug Discovery and Development Settings. *Adv. Drug Delivery Rev.* **2001**, *46* (1−3), 3−26.

(18) Huang, A. H. C. Plant Lipid Droplets and Their Associated Proteins: Potential for Rapid Advances. *Plant Physiol.* **2018**, *176* (3), 1894−1918.

(19) Chen, M. C. M.; Chyan, C.-L.; Lee, T. T. T.; Huang, S.-H.; Tzen, J. T. C. Constitution of Stable Artificial Oil Bodies with Triacylglycerol, Phospholipid, and Caleosin. *J. Agric. Food Chem.* **2004**, *52* (12), 3982−3987.

(20) Gandhi, S. A.; Parveen, S.; Alduhailan, M.; Tripathi, R.; Junedi, N.; Saqallah, M.; Sanders, M. A.; Hoffmann, P. M.; Truex, K.; Granneman, J. G.; Kelly, C. V. Methods for Making and Observing Model Lipid Droplets. *Cell Rep. Methods* **2024**, *4*, No. 100774.

(21) Julien, J. A.; Pellett, A. L.; Shah, S. S.; Wittenberg, N. J.; Glover, K. J. Preparation and Characterization of Neutrally-Buoyant Oleosin-Rich Synthetic Lipid Droplets. *Biochim. Biophys. Acta Biomembr.* **2021**, *1863* (8), No. 183624.

(22) Feng, S.; Kong, L.; Gee, S.; Im, W. Molecular Condensate in a Membrane: A Tugging Game between Hydrophobicity and Polarity with Its Biological Significance. *Langmuir* **2022**, *38* (19), 5955−5962.

(23) Gee, S.; Glover, K. J.; Wittenberg, N. J.; Im, W. CHARMM-GUI Membrane Builder for Lipid Droplet Modeling and Simulation. *ChemPlusChem* **2024**, *89*, No. e202400013.

(24) Zoni, V.; Khaddaj, R.; Campomanes, P.; Thiam, A. R.; Schneiter, R.; Vanni, S. Pre-Existing Bilayer Stresses Modulate Triglyceride Accumulation in the ER versus Lipid Droplets. *eLife* **2021**, *10*, No. e62886.
(25) Barry, N. P. E.; Therrien, B. Pyrene: The Guest of Honor. In *Organic Nanoreactors*; Sadjadi, S., Ed.; Academic Press: Boston, 2016; pp 421−461.
(26) Julien, J. A.; Mutchek, S. G.; Wittenberg, N. J.; Glover, K. J. Biophysical Characterization of Full-Length Oleosin in Dodecylphosphocholine Micelles. *Proteins* **2022**, *90*, 560−565.
(27) Pastor, R. W.; MacKerell, A. D., Jr. Development of the CHARMM Force Field for Lipids. *J. Phys. Chem. Lett.* **2011**, *2* (13), 1526−1532.
(28) Wu, E. L.; Cheng, X.; Jo, S.; Rui, H.; Song, K. C.; Dávila-Contreras, E. M.; Qi, Y.; Lee, J.; Monje-Galvan, V.; Venable, R. M.; Klauda, J. B.; Im, W. CHARMM-GUI Membrane Builder toward Realistic Biological Membrane Simulations. *J. Comput. Chem.* **2014**, *35* (27), 1997−2004.
(29) Jo, S.; Kim, T.; Im, W. Automated Builder and Database of Protein/Membrane Complexes for Molecular Dynamics Simulations. *PLoS One* **2007**, *2* (9), No. e880.
(30) Jo, S.; Lim, J. B.; Klauda, J. B.; Im, W. CHARMM-GUI Membrane Builder for Mixed Bilayers and Its Application to Yeast Membranes. *Biophys. J.* **2009**, *97* (1), 50−58.
(31) Campomanes, P.; Prabhu, J.; Zoni, V.; Vanni, S. Recharging Your Fats: CHARMM36 Parameters for Neutral Lipids Triacylglycerol and Diacylglycerol. *Biophys. Rep.* **2021**, *1* (2), No. 100034.
(32) Jo, S.; Kim, T.; Iyer, V. G.; Im, W. CHARMM-GUI: A Web-Based Graphical User Interface for CHARMM. *J. Comput. Chem.* **2008**, *29* (11), 1859−1865.
(33) Jorgensen, W. L.; Chandraskhar, J.; Madura, J. D.; Impey, R. W.; Klein, M. L. Comparison of Simple Potential Functions for Simulating Liquid Water. *J. Chem. Phys.* **1983**, *79*, 926−935.
(34) Eastman, P.; Galvelis, R.; Peláez, R. P.; Abreu, C. R. A.; Farr, S. E.; Gallicchio, E.; Gorenko, A.; Henry, M. M.; Hu, F.; Huang, J.; Krämer, A.; Michel, J.; Mitchell, J. A.; Pande, V. S.; Rodrigues, J. P.; Rodriguez-Guerra, J.; Simmonett, A. C.; Singh, S.; Swails, J.; Turner, P.; Wang, Y.; Zhang, I.; Chodera, J. D.; De Fabritiis, G.; Markland, T. E. OpenMM 8: Molecular Dynamics Simulation with Machine Learning Potentials. *J. Phys. Chem. B* **2024**, *128* (1), 109−116.
(35) Steinbach, P. J.; Brooks, B. R. New Spherical-Cutoff Methods for Long-Range Forces in Macromolecular Simulations. *J. Comput. Chem.* **1994**, *15*, 667−683.
(36) Åqvist, J.; Wennerström, P.; Nervall, M.; Bjelic, S.; Brandsdal, B. O. Molecular Dynamics Simulations of Water and Biomolecules with a Monte Carlo Constant Pressure Algorithm. *Chem. Phys. Lett.* **2004**, *384* (4), 288−294.
(37) Ryckaert, J.; Ciccotti, G.; Berendsen, H. J. C. Numerical Integration of the Cartesian Equations of Motion of a System with Constraints: Molecular Dynamics of n-Alkanes. *J.Comp.Phys.* **1977**, *23*, 327−341.
(38) Gao, Y.; Lee, J.; Smith, I. P. S.; Lee, H.; Kim, S.; Qi, Y.; Klauda, J. B.; Widmalm, G.; Khalid, S.; Im, W. CHARMM-GUI Supports Hydrogen Mass Repartitioning and Different Protonation States of Phosphates in Lipopolysaccharides. *J. Chem. Inf. Model.* **2021**, *61* (2), 831−839.
(39) Humphrey, W.; Dalke, A.; Schulten, K. VMD: Visual Molecular Dynamics. *J. Mol. Graph.* **1996**, *14* (1), 33−38.
(40) Brooks, B. R.; Brooks, C. L., 3rd; Mackerell, A. D., Jr; Nilsson, L.; Petrella, R. J.; Roux, B.; Won, Y.; Archontis, G.; Bartels, C.; Boresch, S.; Caflisch, A.; Caves, L.; Cui, Q.; Dinner, A. R.; Feig, M.; Fischer, S.; Gao, J.; Hodoscek, M.; Im, W.; Kuczera, K.; Lazaridis, T.; Ma, J.; Ovchinnikov, V.; Paci, E.; Pastor, R. W.; Post, C. B.; Pu, J. Z.; Schaefer, M.; Tidor, B.; Venable, R. M.; Woodcock, H. L.; Wu, X.; Yang, W.; York, D. M.; Karplus, M. CHARMM: The Biomolecular Simulation Program. *J. Comput. Chem.* **2009**, *30* (10), 1545−1614.

https://doi.org/10.1021/acsomega.4c07512
ACS Omega 2024, 9, 43193−43202